

Exposure Bias Reduction for Enhancing Diffusion Transformer Feature Caching

Zhen Zou, Hu Yu, Jie Xiao, Feng Zhao
University of Science and Technology of China

{zouzhen, yuhu520, ustchbxj}@mail.ustc.edu.cn, fzha0956@ustc.edu.cn

Abstract

Diffusion Transformer (DiT) has exhibited impressive generation capabilities but faces great challenges due to its high computational complexity. To address this problem, various methods, notably feature caching, have been introduced. However, these approaches focus on aligning non-cache diffusion without analyzing the impact of caching on the generation of intermediate processes. So the lack of exploration provides us with room for analysis and improvement. In this paper, we analyze the impact of caching on the SNR of the diffusion process and discern that feature caching intensifies the denoising procedure, and we further identify this as a more severe exposure bias issue. Drawing on this insight, we introduce EB-Cache, a joint cache strategy that aligns the Non-exposure bias (which gives us a higher performance ceiling) diffusion process. Our approach incorporates a comprehensive understanding of caching mechanisms and offers a novel perspective on leveraging caches to expedite diffusion processes. Empirical results indicate that EB-Cache optimizes model performance while concurrently facilitating acceleration. Specifically, in the 50-step generation process, EB-Cache achieves $1.49\times$ acceleration with 0.63 FID reduction from 3.69, surpassing prior acceleration methods. Code will be available at <https://github.com/aSleepyTree/EB-Cache>.

1. Introduction

The advent of Diffusion Transformer (DiT) [32] has catalyzed the generative modeling field, particularly in image [11, 13, 34] and video generation [4]. DiT has showcased an unprecedented ability to synthesize high-fidelity visual content, offering a powerful alternative to previous U-Net architecture diffusion models [8, 13]. However, the remarkable capabilities of DiT are accompanied by a significant computational cost, which becomes increasingly burdensome when tackling large amounts of samples [41]. As a result, the computational cost escalates dramatically with even modest increases in resolution, posing a substantial challenge to the practical deployment of DiTs [5, 6, 25, 33].

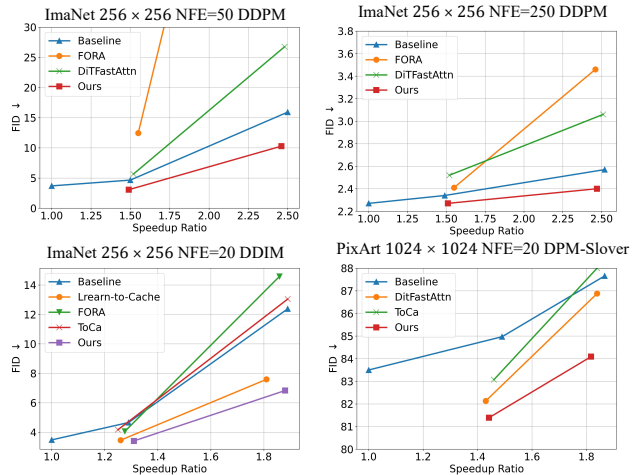


Figure 1. Comparison between our method and other methods. Baseline indicates simply reducing sampling steps.

Feature caching [7, 28, 36, 43] is a common approach to address this challenge. As a pioneer, DeepCache [28] avoids deep-level calculations by caching shallow features in U-Net-based diffusion models. Recently, FORA [36] and Learning-to-Cache (L2C) [27] adapt caching strategy into DiT, yielding commendable results. Feature caching operates on the premise of storing intermediate feature representations for reuse in subsequent diffusion steps, thereby diminishing the need for repetitive and costly calculations. Given the similarity of features between adjacent steps, these methods are intuitively sound and have demonstrated notable acceleration in generative processes.

While feature caching has provided a promising pathway to expedite generation, it has also been observed to compromise the quality of the generated images at times. We posit that this is attributable to these methods concentrating on aligning cached diffusion with the steps of standard diffusion, and they have not explored the operational effect of caching on visual effects. Therefore, we believe that delving into the statistical results of the above visual effects could bring a new view to understand feature caching, leading to a new potential design of cache strategies.

Our analysis begins with the visual effects that **images**

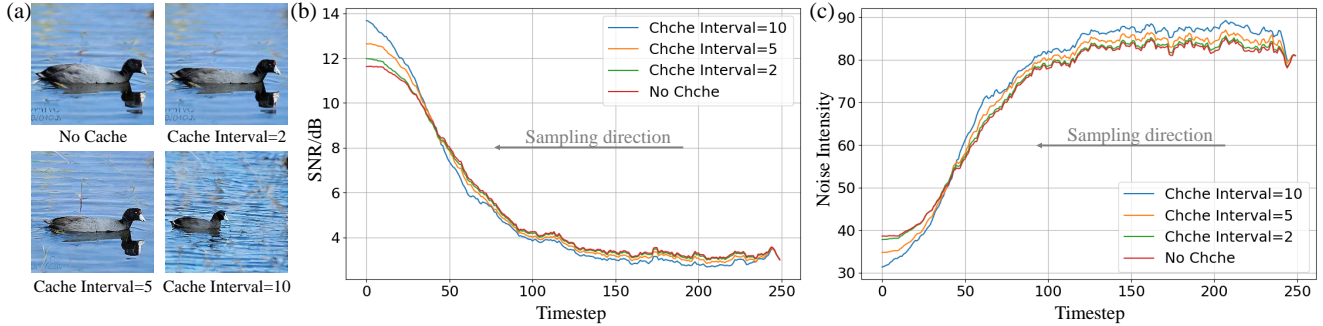


Figure 2. (a) Images generated with larger intervals tend to be sharper. (b) SNR of different cache intervals during the diffusion process. **Feature caching elevates SNR.** Note that calculations are performed in image space decoded by VAE [17]. (c) Noise of different cache intervals. **Feature caching reduces image noise.** Refer to Sec. 3.1 for detailed analysis.

generated with feature caching tend to be sharper as shown in Fig. 2(a). This prompts us to observe the SNR of images throughout the denoising process. What we find interesting in Fig. 2(b) is that caching elevates the SNR of images. This indicates that *caching intensifies the network’s denoising capabilities*, potentially causing the network to remove excessive noise and thus divert the diffusion process from its trajectory. Further analysis in Fig. 2(c) reveals that caching results in smaller noise intensity compared to the No-cache scenario, confirming our conjecture.

The observation of noise intensity alerted us about exposure bias, a phenomenon that comes from the discrepancy between training and testing phases of diffusion models, also *induces the network to predict a slightly larger noise*. We have observed that similar to feature caching, the amplification of exposure bias is accompanied by an increase in image SNR, as shown in Fig. 3(a). It naturally occurs to us that feature caching would lead to a more severe exposure bias issue. Thus, connecting feature caching with exposure bias reduction could potentially eliminate the weakness of caching with approaches used to address exposure bias.

In this paper, we demonstrate that caching exacerbates exposure bias. Based on this insight, we propose *Exposure Bias-based Cache* (EB-Cache) to manage exposure bias flexibly while achieving acceleration. Our approach is predicated on aligning with non-exposure-bias diffusion, where caching plays a dual role in both fitting exposure bias and enabling acceleration. We design the cache strategy in two levels: step-wise and structure-wise (as shown in Fig. 4). The step-wise design introduces an adaptive Cache Table, which meets the non-uniformity across time steps to counterbalance the uneven distribution of exposure bias in caching: substantial cache amplification is applied where exposure bias is minimal, and no cache is utilized where exposure bias is severe. The additional noise scaling balances the exposure bias throughout the entire diffusion process. For structure-wise, we differentiate between self-attention and feedforward networks, noting their distinct varying de-

grees of similarities and cacheability, leading us to adopt separate caching strategies for them under the Cache Table. We summarize our contributions as follows:

- We analyze the visual effect of feature caching and find that caching intensifies the denoising procedure, which caters to a more severe exposure bias issue of generation.
- Instructed by exposure bias, we design a versatile cache strategy from the step-wise and structure-wise levels with exposure bias reduction during generation.
- Extensive experiments demonstrate the effectiveness and reliability of our method in different scenarios. Moreover, our method can be plugged into existing caching approaches to further boost their performance.

2. Related Work

2.1. Acceleration of Diffusion Transformers

Diffusion model’s huge computational burden comes from its iterative denoising during the inference process, which can’t be performed in parallel due to the Markov chain [13]. A variety of acceleration techniques have been proposed to overcome this challenge [2, 3, 10, 22, 37, 38, 46, 47]. Some methods rely on model compression or quantization to reduce the model size or computational accuracy [9, 15, 26, 35, 37, 38]. In addition, some methods explore efficient solvers and strategies to minimize the steps required to generate high-quality images [14, 21, 23, 24, 39, 48].

Another way is to reduce the average amount of calculation per step [19, 44]. Some works [7, 27, 36] introduce the idea of feature caching and adapt it to the transformer architecture. FORA [36] replaces layers with the output of previous step. Δ -DiT [7] skips layers by caching feature residuals instead of feature maps. Reusing similar features significantly reduces computational costs.

The success of the cache-based method comes from the high similarity between the features of adjacent steps [27, 36]. However, this similarity is not absolute. Blind reuse will make the model insensitive to the data distribu-

tion of the sampling process, which may cause the loss of key details and ultimately lead to failure cases. Unfortunately, the above studies apply feature cache based on similar features, without exploring the reasons why cache damages quality or a fundamental principle to guide the application of cache. In this paper, we explore the reasons why feature caching damages generation quality and flexibly apply cache strategies under the guidance of this principle.

2.2. Exposure Bias in Diffusion Models

Exposure bias in Diffusion Models is a significant issue that has attracted considerable research attention in the field of generative modeling [18, 29, 30, 40]. Exposure bias refers to the discrepancy between the training and inference processes of a model, which can lead to suboptimal performance during generation. In the context of DPMS, this bias is exacerbated by the fact that the models typically require numerous iterative steps to synthesize high-quality images, making the models prone to accumulate errors to an explosion during the inference process.

Some methods have been proposed to solve this problem. Li et al. [18] believe that although there is a deviation between the prediction of \hat{x}_0^t and the ground truth x_0 , there may be another $\hat{x}_0^{t_s}$ better coupled with x_0 . The authors propose a Time-Shift Sampler to search for such t_s around t to avoid exposure bias. Ning et al. [29] find that exposure bias makes the network predict *slightly too much noise* and thus impairs the network performance. The authors propose a method named Epsilon Scaling to weaken this effect by scaling the prediction noise of the network. However, since the influence of exposure bias is uneven throughout the diffusion process, determining hyperparameters remains a problem. **In this paper, we modulate exposure bias with feature caching, achieving a uniform exposure bias throughout the diffusion process, which can be dealt with a constant scaling parameter.**

3. Motivation

3.1. Feature Caching in Diffusion Transformers

Modern feature caching methodologies leverage inter-step feature similarity to accelerate generation. Representative work like FORA [36] employs fixed-interval caching based on high feature correlation between consecutive steps. While these methods attempt to align cached steps with original diffusion dynamics through synchronization mechanisms, two fundamental limitations persist: (1) Performance remains bounded by the basic diffusion model’s capability, and (2) The inherent computational discrepancy between cached and regular steps creates optimization barriers. More critically, existing approaches inadequately explore caching’s statistical impacts on signals like SNR.

Our observations(Fig. 2(a)) and signal-processing per-

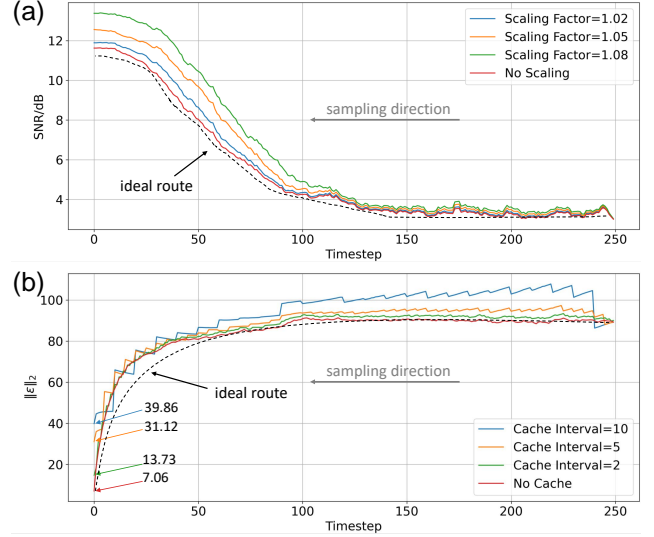


Figure 3. (a) For ease of observation, we use factors larger than 1 to amplify exposure bias. Exposure bias causes SNR to rise. (b) Feature caching results in greater exposure bias. The intensity of amplification is related to the interval.

spective analysis(Fig. 2(b)) reveal counterintuitive caching effects: even limited caching increases image SNR, suggesting enhanced denoising capability contradicting conventional assumptions. Noise intensity distribution corresponding to Figure 2(b) in Fig. 2(c) quantifies this phenomenon, demonstrating noise reduction. The underlying mechanism stems from temporal misalignment in cached diffusion. Early-stage denoising typically eliminates significant noise, but caching-induced latency applies historical denoising intensities to current steps [12, 16, 20, 29]. This mismatch creates cascading effects resembling exposure bias - the training-inference discrepancy fundamental to diffusion models. Our analysis bridges these phenomena through their shared statistical distortion characteristics.

3.2. Exposure Bias in Feature Caching

Exposure bias comes from the inconsistency between training and inference phases in diffusion models. Follow [29], the prediction error between the estimated \hat{x}_0^{t-1} and ground truth x_0 at step t can be formulated as:

$$\hat{x}_0^{t-1} = x_0 + e_{t-1}\epsilon_0 \quad (\epsilon_0 \sim \mathcal{N}(0, I)), \quad (1)$$

where e_{t-1} represents the error magnitude, and ϵ_0 denotes standard Gaussian noise. This prediction error propagates through the reverse process, resulting in the perturbed sample at step $t - 1$:

$$\hat{x}_{t-1} = \sqrt{\bar{\alpha}_{t-1}}x_0 + \sqrt{1 - \bar{\alpha}_{t-1} + \underbrace{\left(\frac{\sqrt{\bar{\alpha}_{t-1}}\beta_t}{1 - \bar{\alpha}_t}\right)^2}_{\text{Exposure Bias Term}}}e_1, \quad (2)$$

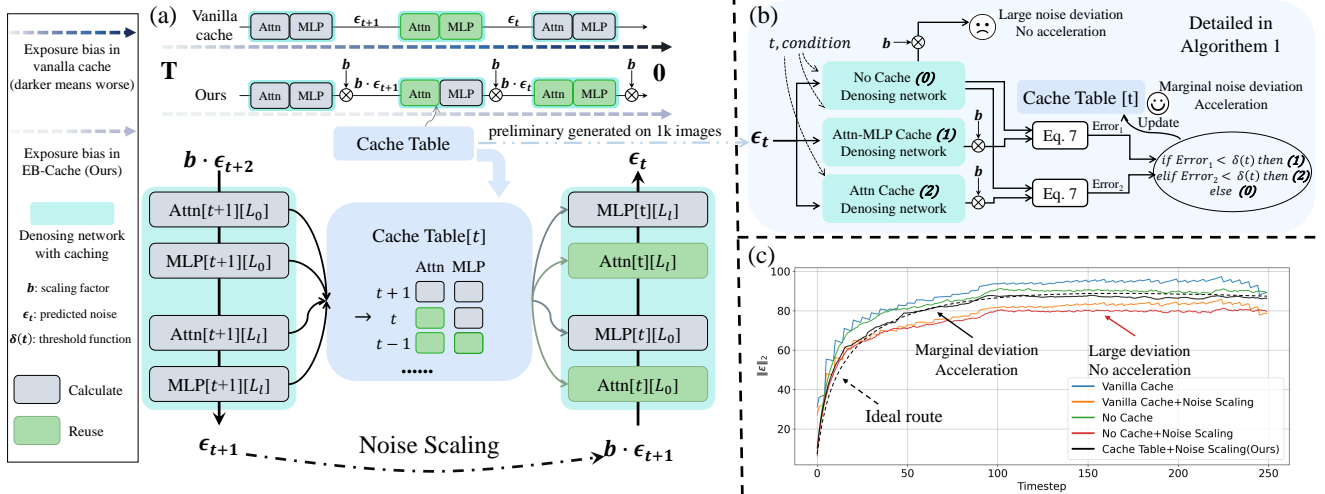


Figure 4. (a) Illustration of EB-Cache. EB-Cache achieves less exposure bias while speeding up. Cache Table is preliminarily generated with (b) on 1k images. (c) Noise Scaling exhibits a large deviation and no acceleration without Cache Table. Our method achieves marginal deviation and acceleration with Cache Table+Noise Scaling.

where $\bar{\alpha}_{t-1}$ and β_t denote noise schedule parameters in diffusion process, and the exposure bias term originates from the prediction error in Eq. 1.

Feature caching reuses intermediate features from step $t-1$ in subsequent step $t-2$, effectively superimposing similar error distributions. Under the extreme (but analytically useful) assumption of identical error distributions:

$$\hat{x}_0^{t-2} = \hat{x}_0^{t-1} + e_{t-1}\epsilon_0 = x_0 + 2e_{t-1}\epsilon_0. \quad (3)$$

This error superposition transforms additive variance accumulation ($\propto N$) into quadratic growth ($\propto N^2$) over N steps. Substituting Eq. 3 into Eq. 2 and extending to $t-N$:

$$\hat{x}_{t-N} = \sqrt{\bar{\alpha}_{t-N}}x_0 + \sqrt{1 - \bar{\alpha}_{t-N} + N^2 \left(\frac{\sqrt{\bar{\alpha}_{t-N}}\beta_{t-N+1}}{1 - \bar{\alpha}_{t-N+1}} e_t \right)^2} \epsilon_2. \quad (4)$$

This quadratic scaling (N^2 vs. the baseline N in No-cache scenarios) quantifies how feature caching amplifies inherent exposure bias. As $\|\epsilon\|_2$ curves visualized in Fig. 3(b), caching exacerbates noise amplification of exposure bias, leading to controllable sampling offsets in standard diffusion processes to a non-negligible problem. Refer to supplementary material for complete derivation and general analysis with relaxed assumptions (intensification is not as dramatic as N^2 , but it's still superlinear).

3.3. Modulate Exposure Bias with Feature Caching

Our analysis reveals a critical insight: **feature caching in the diffusion process intensifies exposure bias, increasing predicted noise**(Fig. 2 and 3). This interaction establishes feature caching as a dynamic control tool for exposure bias modulation, which indicates that exposure bias can be smoothed and then addressed.

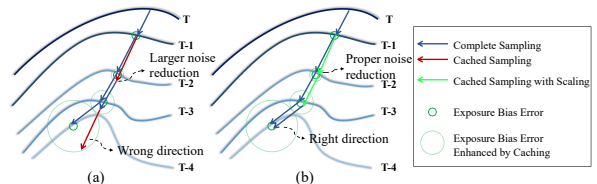


Figure 5. Standard cache (a) predicts larger noise (amplification of exposure bias) and does not perceive the change of denoising direction. Our method (b) scales the noise to keep the exposure bias error within an acceptable range. Cache Table senses direction changes and corrects.

A promising solution to address exposure bias was proposed by Ning et al. [29], who claimed that scaling the noise of diffusion models could mitigate this issue. They utilize static scaling factors paired with manual searching. **However, since the severity of exposure bias varies dynamically across the diffusion process, the static scaling strategy fails to achieve optimal adaptation.** Specifically, exposure bias exhibits a temporally uneven distribution. Early stages: the cumulative impact of exposure bias remains negligible, requiring minimal intervention. Middle stages: accumulated deviations grow substantially, degrading generation quality and necessitating targeted mitigation [18, 29]. Final stages: as the model focuses on fine-grained details, aggressive corrections risk over-regularization and distortion of high-frequency features [7, 13].

Leveraging adaptive feature caching as a dynamic instrument to smooth exposure bias, we employ noise scaling to achieve a synergistic removal. This can be explained as **using feature caching at appropriate steps to intensify exposure bias to construct a smoothed effect over all timesteps so that it can be eliminated by a static**

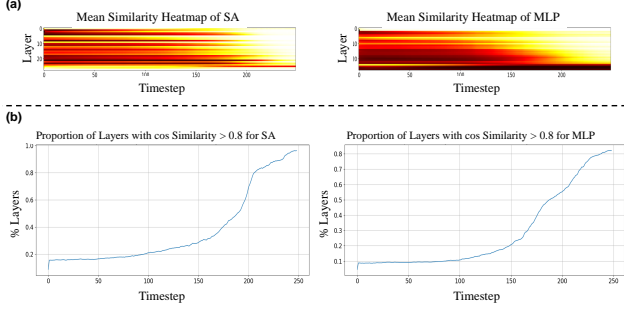


Figure 6. **Separate feature similarity analysis of self-attention and MLP.** (a) Similarity heat map. A lighter color indicates higher similarity. (b) Proportion for high similarity layers. Higher similarities in SA than MLP.

noise reduction. Based on this insight, we propose a dual-component caching strategy integrating *noise scaling* and *adaptive feature caching* that simultaneously enhances generation quality and boosts computational efficiency. We present a comparative visualization in Fig. 5.

4. Method

4.1. Caching for Better Exposure Bias Reduction

Our method revolves around three pivotal components: **Noise Scaling** ($\epsilon_t \rightarrow b \cdot \epsilon_t$): Over-corrected exposure bias gives a buffer for feature caching to smooth it.

Cache Table: It’s generated via precomputation over 1k representative samples using Algorithm 1.

Cache Candidates: Candidates comprise three modes:

- ATTN-MLP CACHE: full module reuse
- ATTENTION CACHE: attention reuse only
- NO CACHE: baseline computation

MLP CACHE is omitted due to suboptimal performance. Reasons will be introduced in Sec. 4.2.

As illustrated in Fig. 4(a), for DiT blocks at step $t + 1$:

$$F_{mid} = Attn(I(t + 1)) + I(t + 1), \quad (5)$$

$$F_{out} = F_{mid} + MLP(F_{mid}), \quad (6)$$

where we omit components such as layer norm. We store $Attn(I(t + 1))$ and $MLP(F_{mid})$ for all layers in normally calculated steps and then replace the corresponding self-attention or MLP output according to Cache Table in the next steps. We do not assign a separate cache strategy to each layer because of the coupling effect between layers.

A heuristic search algorithm is used to determine Cache Table as shown in Algorithm 1 and Fig. 4(b). First, we get the outputs of candidate cache strategies and calculate their respective L2-norms marked as $E_{candidate}(t)$. Errors between original and cached outputs are then calculated with:

$$Error = \|E_{ori}(t) - E_{candidate}(t)\|_1. \quad (7)$$

Algorithm 1 Cache Table Generation

```

1: Input: Denoising Network  $\epsilon_\theta$ , Scaling Factor  $b$ , Total Step  $T$ , Error Threshold Function  $\delta(t)$ 
2: Initialize Cache Table  $\leftarrow \emptyset$ 
3: repeat
4:    $x_T \sim \mathcal{N}(0, I)$ 
5:    $x_{T-1} = \frac{1}{\sqrt{\alpha_T}}(x_T - \frac{\beta_T}{\sqrt{1-\alpha_T}}\epsilon_\theta(x_T, T) \cdot b)$ 
6:   for  $t := T - 2, \dots, 1$  do
7:      $E_{ori}(t) \leftarrow \|\epsilon_\theta(x_t, t)\|_2$ 
8:      $E_{Attn-MLP}(t) \leftarrow \|b \cdot \epsilon'_\theta(x_t, t)\|_2$ 
9:      $E_{Attn}(t) \leftarrow \|b \cdot \epsilon''_\theta(x_t, t)\|_2$ 
10:    if  $\|E_{ori}(t) - E_{Attn-MLP}(t)\|_1 < \delta(t)$  then
11:      Tag  $t$ : ATTN-MLP CACHE
12:    else if  $\|E_{ori}(t) - E_{Attn}(t)\|_1 < \delta(t)$  then
13:      Tag  $t$ : ATTENTION CACHE
14:    else
15:      Tag  $t$ : NO CACHE
16:    end if
17:  end for
18: until 1k iterations
19: Weight Cache Table

```

Then the strategy with *Error* less than threshold $\delta(t)$ and the largest speedup is selected into Cache Table. The Cache Table will be weighted after 1k iterations. Taking sampling 50,000 images as an example, time spent on generating Cache Table is on average less than $\frac{1}{30}$ of total sampling time (FLOPs(P): 8.97 vs 296.43, Latency(s): 197 vs 6059). The threshold is a linear function proportional to timesteps. for instance: $\delta(t) = 0.05 + 0.15 \cdot \frac{t}{T}$, $t \in [0, T)$.

4.2. Separate Caching for Attention and MLP

Previous studies [1, 31, 42] have highlighted that the self-attention mechanism within Transformers predominantly filters low-frequency information, while the MLP processes high-frequency information more extensively. Recognizing the distinct roles of these components may influence their cacheability within the DiT architecture. To explore this, we visualized the cosine similarity of self-attention and MLP outputs across consecutive steps in DiT/XL and calculated the percentage of layers exceeding a similarity threshold of 0.8, as depicted in Fig. 6. The visualization reveals that the self-attention heatmap is generally lighter, indicating a higher degree of similarity among layers compared to the MLP. Specifically, for any given step, self-attention exhibits a greater proportion of layers with high similarity. Please refer to the supplementary material for more information.

This observation suggests that self-attention mechanisms possess superior cacheability characteristics. Consequently, this insight steers us toward designing cache structures that go beyond the temporal dimension of timesteps. By doing so, we can enhance the efficiency of feature caching,

Table 1. Comparison on ImageNet with DiT/XL-2 DDPM. Note that L2C degenerates to FORA when speedup ratio > 2 .

Methods	NFE	FLOPs(T)	Latency(s)	Speedup	FID↓	sFID↓	IS↑	Precision↑	Recall↑
DiT-XL/2 (ImageNet 256×256) (cfg=1.5)									
DiT [32]	250	29.67	77.42	1.00	2.27	4.62	279.36	0.83	0.57
DiT [32]	165	19.58	51.36	1.51	2.36	5.11	265.71	0.81	0.57
FORA(N=2) [36]	250	16.27	49.96	1.55	2.41	5.38	266.81	0.81	0.59
DiTFastAttn [46]	250	16.40	50.90	1.52	2.52	5.03	269.58	0.82	0.58
L2C [27]	250	20.18	57.35	1.35	2.31	4.90	271.97	0.81	0.58
Ours	250	16.53	50.52	1.53	2.27	4.91	273.09	0.82	0.59
DiT [32]	100	11.93	30.96	2.50	2.57	5.73	251.69	0.81	0.57
FORA(N=4) [36]	250	11.31	31.49	2.46	3.46	8.06	243.17	0.78	0.59
DiTFastAttn [46]	250	11.40	30.21	2.51	3.06	7.43	253.09	0.79	0.56
ToCa(N=4,R=90%) [50]	250	11.87	31.79	2.44	2.52	5.40	260.19	0.81	0.58
ToCa + Ours	250	11.36	30.90	2.51	2.43	5.29	260.97	0.81	0.58
Ours	250	11.73	31.27	2.48	2.40	5.16	263.91	0.81	0.58
DiT [32]	50	5.98	15.52	1.00	3.69	8.56	220.05	0.78	0.57
DiT [32]	33	3.87	10.37	1.50	4.65	8.56	197.02	0.78	0.57
FORA(N=2) [36]	50	3.51	10.01	1.55	8.45	14.28	178.93	0.80	0.56
DiTFastAttn [46]	50	3.66	10.21	1.52	5.66	10.34	164.11	0.79	0.56
L2C [27]	50	4.03	11.91	1.30	3.73	8.61	209.88	0.80	0.57
Ours	50	3.49	10.40	1.49	3.06	5.97	216.89	0.80	0.57
DiT [32]	20	2.47	6.20	2.50	15.92	19.22	173.58	0.78	0.57
FORA(N=4) [36]	50	2.39	6.34	2.45	88.21	102.40	100.03	0.51	0.46
DiTFastAttn [46]	50	2.43	6.33	2.45	61.07	70.05	101.74	0.61	0.52
ToCa(N=4,R=90%) [50]	50	2.51	6.47	2.40	13.77	20.10	177.60	0.73	0.57
ToCa + Ours	50	2.43	6.28	2.47	13.10	18.52	181.72	0.73	0.57
Ours	50	2.40	6.30	2.46	10.28	15.92	196.83	0.76	0.58
DiT-XL/2 (ImageNet 512×512) (cfg=1.5)									
DiT [32]	100	11.87	88.73	1.00	5.83	17.30	213.57	0.83	0.63
DiT [32]	60	7.28	53.75	1.65	6.10	17.21	206.15	0.83	0.62
FORA(N=2) [36]	100	7.33	53.28	1.67	6.36	19.20	202.90	0.84	0.65
DiTFastAttn [46]	100	7.27	53.88	1.65	6.10	19.13	208.80	0.83	0.64
L2C [27]	100	7.15	54.62	1.63	6.01	17.56	208.38	0.84	0.64
ToCa(N=3,R=70%) [50]	100	7.40	54.93	1.62	6.04	17.29	206.90	0.83	0.63
ToCa + Ours	100	7.17	53.29	1.67	5.97	17.11	208.99	0.83	0.65
Ours	100	7.20	52.37	1.69	5.93	16.81	210.33	0.84	0.65

Table 3. PixArt- Σ T2I generation.

1024 × 1024 PixArt- Σ DPM-Solver					
Methods	FLOPs(T)	Latency(s)	FID ↓	CLIP ↑	IS ↑
PixArt- Σ (T=20) [6]	173.08	1.39	83.50	32.01	23.61
PixArt- Σ (T=13) [6]	112.52	0.93	84.97	31.84	23.10
ToCa (N = 3, R = 50%) [50]	109.93	0.95	83.07	32.10	23.41
DiTFastAttn [46]	113.00	0.97	82.06	31.99	23.17
Δ -DiT [7]	112.25	0.95	82.72	32.03	23.67
Ours	113.52	0.97	81.39	32.29	23.88
2048 × 2048 PixArt- Σ DPM-Solver					
PixArt- Σ (T=20) [6]	693.88	5.39	139.79	37.81	21.07
PixArt- Σ (T=13) [6]	450.01	3.67	143.69	37.19	20.49
ToCa (N = 3, R = 50%) [50]	428.93	3.62	140.77	37.57	21.05
DiTFastAttn [46]	451.33	3.79	138.67	37.69	21.01
Δ -DiT [7]	446.29	3.78	141.80	37.66	20.94
Ours	449.37	3.73	139.17	38.02	21.20

Table 4. 720 × 480 CogVideoX-2B T2V generation.

Methods	FLOPs(T)	Latency(s)	VBench(%) ↑	PSNR ↑	SSIM ↑	LPIPS ↓
CogVideoX (T=50) [45]	8417.40	142.10	80.91	-	-	-
CogVideoX (T=35) [45]	5892.18	98.73	78.19	25.70	0.9183	0.0541
PAB ₃₅₇ [49]	5905.38	97.52	78.66	25.48	0.9213	0.0529
Δ -DiT [7]	5861.42	96.61	78.21	25.51	0.9207	0.0537
Ours	5910.74	98.01	78.83	25.66	0.9225	0.0515

thereby improving the overall generation process.

5. Experiment

This section presents an overview of our experimental setup, including datasets, evaluation models, experimental configurations, and assessment metrics used and results.

Table 2. 256 × 256 ImageNet DiT-XL/2 with DDIM.

Methods	FLOPs(T)	Latency(s)	FID ↓	sFID ↓	IS ↑
DiT (T=20) [32]	2.37	5.93	3.48	4.88	222.97
DiT (T=16) [32]	1.90	4.63	4.66	5.71	209.72
ToCa (N=2, R=40%) [50]	1.88	4.73	4.17	5.13	213.01
DiTFastAttn [46]	1.88	4.67	4.09	5.21	219.30
Δ -DiT [7]	1.91	4.61	3.97	5.19	211.62
L2C [27]	1.86	4.69	3.46	4.66	226.76
Ours	1.88	4.61	3.41	4.64	224.43



Figure 7. Qualitative comparison on ImageNet 256×256 with 50 and 100 NFEs.

5.1. Experimental Settings and Baselines

We explore our methods on the most used transformer-based diffusion model: DiT with different NFEs. Following [27], we test DiT-XL/2 (256×256) with 50 and 250 NFEs and DiT-XL/2 (512×512) with 100 NFEs on ImageNet. Settings are consistent with standard DiT. DDIM works well with few steps, so we test it with 20 NFEs in Tab. 2. In order to verify the generalizability of EB-Cache in more complex models and tasks, we perform experiments with pixArt- Σ [6] for T2I and CogvideoX [45] for T2V. Baselines include FORA [36], Δ -DiT [7], L2C [27], DiTFastAttn [46], ToCa [36], and PAB [49]. Some methods are not suitable for certain acceleration ratios and tasks or perform poorly due to parameter issues. Refer to supplementary material for complete comparisons.

5.2. Main Results

We present the experimental results in Tab. 1, 2, 3 and 4. In general, EB-Cache perfectly achieves a balance between speed and quality. For example, in 50 steps of generation on ImageNet 256×256 , our approach achieves a $1.49 \times$ acceleration and an FID of 3.06, which is not only better than the unaccelerated DiT but also better than 3.39 of DiT+Epsilon Scaling[29] (not shown in the table). This is because the flexible cache strategy makes up for the over-correction of noise caused by Epsilon Scaling in some steps. Original Ep-



Figure 8. Qualitative comparison on PixArt- Σ .

silon Scaling on DiT uses a fixed scaling factor throughout the generation process, while our heuristic cache strategy makes up for this deficiency of Epsilon Scaling in specific steps by exploiting the amplification effect of cache on exposure bias. We show some samples in Fig. 7 and 8 and more visualization including video samples can be found in the supplementary material.

5.3. Ablation Study

In this section, we conduct an ablation study on our method to verify its robustness by examining two adjustable hyper-parameters: the scaling factor and the threshold function.

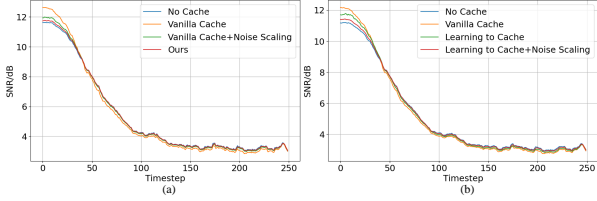


Figure 9. (a) Simply scaling the noise helps vanilla cache align with No-cache. Our method does a better job. (b) L2C also shows a tendency to align No-cache on SNR.

Table 5. Ablation on scaling factors.

scaling factor	baseline	0.945	0.950	0.955(Ours)	0.960	0.965
FID ↓	4.65	3.35	3.27	3.06	3.21	3.42
IS ↑	197.02	213.9	215.14	216.89	214.99	213.73

Table 6. Ablation on type of threshold functions.

functions	baseline	Positive Linear(Ours)	Negative Linear	Uniform
FID ↓	2.36	2.27	2.43	2.31
IS ↑	265.71	273.09	261.77	271.83

Table 7. Ablation on parameter of threshold functions.

(a, b)	baseline	(0.1, 0.05)	(0.05, 0.15)	(0, 0.25)
FID ↓	2.36	2.32	2.27	2.35
IS ↑	265.71	266.09	273.09	269.44

Choice of Scaling Factor: We illustrate the impact of different scaling factors in Tab. 5. Since subsequent Cache Table searching effectively compensates for variations in the scale factor, our method demonstrates robustness across scale values. In practice, we determine scaling factors by searching within an empirical range.

Influence of Threshold Function: In Tab. 6 and 7 we show the effects of different threshold function types and parameters ($\delta(t) = a + b \cdot \frac{t}{T}, t \in [0, T)$). Beyond erroneous function forms (e.g., negative-linear violating commonly assumed degree of noise tolerance of the diffusion process), our method demonstrates robustness, with different settings consistently outperforming baseline approaches.

5.4. Analysis

To verify our initial conjecture, we show the SNR curve of uniform caching in Fig. 9(a). Although not as good as our method, noise scaling for vanilla cache also shows a better SNR. In addition, in Fig. 9(b) we find that L2C also outperforms vanilla cache, showing a tendency to align No-cache on SNR. At the same time, suitable noise reduction can further improve L2C. We visualized the feature errors at the intermediate step versus the No-cache version in Fig. 10. The error of EB-Cache and GT is only reflected in edges and the absolute error is marginal, while the vanilla cache has a large error in the structure, which deviates from the ideal sampling. More analysis can be found in supplementary material.

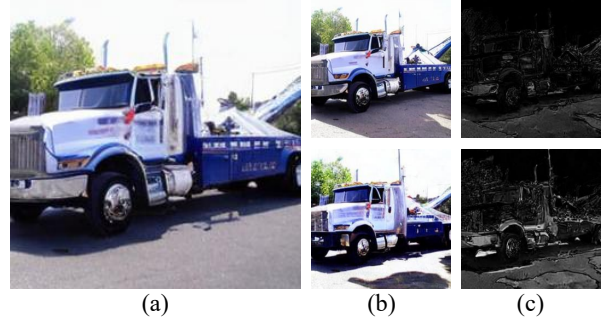


Figure 10. Feature error visualization. (a) Ground truth. (b) Samples generated by *top*: Ours and *bottom*: Vanilla cache. (c) Feature error between Ground truth and *top*: Ours and *bottom*: Vanilla cache at step 20. Our method shows lower errors in features.

Table 8. FLOPs and time analysis in DiT/XL

	Self-Attention	MLP	Other Components
FLOPs	38%	62%	-
Time Proportion	51%	35%	14%

5.5. Quality-Speed Trade Off

In Tab. 8, we analyze the computational overhead and FLOPs of different components in DiT/XL when generating 256px images. Computational overhead is obtained by removing the corresponding component in DiT. Despite the modest FLOPs proportion, self-attention takes approximately $1.5\times$ running timeshare compared to MLP. As aforementioned, Self-attention exhibits higher feature similarity compared to MLP, indicating a greater degree of redundancy. High cacheability is intertwined with high time consumption, so we allocate larger cache intervals to self-attention, which is a pivotal factor contributing to the superior performance of our method over approaches that do not differentiate between self-attention and MLP.

6. Conclusion

In this paper, we point out the reason why DiT acceleration methods based on feature caching fails in quality: it greatly amplifies the exposure bias, and propose a method to achieve a balance between quality and speed with Epsilon Scaling. This is the first exploration in this area, bringing a new perspective to the community. We propose that separate cache intervals should be applied to the attention and MLP to adapt to the different cacheability of these two. Our method does not require heavy training and can be integrated with fast samplers. Experimental results show that compared with other acceleration strategies applied to DiT, this method is quite competitive and can significantly improve the speed while maintaining good quality.

References

- [1] Jiawang Bai, Li Yuan, Shu-Tao Xia, Shuicheng Yan, Zhifeng Li, and Wei Liu. Improving vision transformers by revisiting high-frequency components. In *European Conference on Computer Vision*, pages 1–18. Springer, 2022. 5
- [2] Daniel Bolya and Judy Hoffman. Token merging for fast stable diffusion. In *Proceedings of the IEEE/CVF conference on computer vision and pattern recognition*, pages 4599–4603, 2023. 2
- [3] Daniel Bolya, Cheng-Yang Fu, Xiaoliang Dai, Peizhao Zhang, Christoph Feichtenhofer, and Judy Hoffman. Token merging: Your vit but faster. *arXiv preprint arXiv:2210.09461*, 2022. 2
- [4] Tim Brooks, Bill Peebles, Connor Holmes, Will DePue, Yufei Guo, Li Jing, David Schnurr, Joe Taylor, Troy Luhman, Eric Luhman, et al. Video generation models as world simulators. 2024. URL <https://openai.com/research/video-generation-models-as-world-simulators>, 3, 2024. 1
- [5] Junsong Chen, Jincheng Yu, Chongjian Ge, Lewei Yao, Enze Xie, Yue Wu, Zhongdao Wang, James Kwok, Ping Luo, Huchuan Lu, et al. Pixart- α : Fast training of diffusion transformer for photorealistic text-to-image synthesis. *arXiv preprint arXiv:2310.00426*, 2023. 1
- [6] Junsong Chen, Chongjian Ge, Enze Xie, Yue Wu, Lewei Yao, Xiaozhe Ren, Zhongdao Wang, Ping Luo, Huchuan Lu, and Zhenguo Li. Pixart- σ : Weak-to-strong training of diffusion transformer for 4k text-to-image generation. *arXiv preprint arXiv:2403.04692*, 2024. 1, 6, 7
- [7] Pengtao Chen, Mingzhu Shen, Peng Ye, Jianjian Cao, Chongjun Tu, Christos-Savvas Bouganis, Yiren Zhao, and Tao Chen. δ -dit: A training-free acceleration method tailored for diffusion transformers. *arXiv preprint arXiv:2406.01125*, 2024. 1, 2, 4, 6, 7
- [8] Prafulla Dhariwal and Alexander Nichol. Diffusion models beat gans on image synthesis. *Advances in neural information processing systems*, 34:8780–8794, 2021. 1
- [9] Zhenyuan Dong and Sai Qian Zhang. Ditas: Quantizing diffusion transformers via enhanced activation smoothing. *arXiv preprint arXiv:2409.07756*, 2024. 2
- [10] Fang Gongfan, Ma Xinyin, and Wang Xinchao. Structural pruning for diffusion models. *arXiv preprint arXiv:2305.10924*, 2023. 2
- [11] Ian Goodfellow, Jean Pouget-Abadie, Mehdi Mirza, Bing Xu, David Warde-Farley, Sherjil Ozair, Aaron Courville, and Yoshua Bengio. Generative adversarial networks. *Communications of the ACM*, 63(11):139–144, 2020. 1
- [12] Tiankai Hang and Shuyang Gu. Improved noise schedule for diffusion training. *arXiv preprint arXiv:2407.03297*, 2024. 3
- [13] Jonathan Ho, Ajay Jain, and Pieter Abbeel. Denoising diffusion probabilistic models. *Advances in neural information processing systems*, 33:6840–6851, 2020. 1, 2, 4
- [14] Tero Karras, Miika Aittala, Timo Aila, and Samuli Laine. Elucidating the design space of diffusion-based generative models. *Advances in neural information processing systems*, 35:26565–26577, 2022. 2
- [15] Bo-Kyeong Kim, Hyoung-Kyu Song, Thibault Castells, and Shinkook Choi. On architectural compression of text-to-image diffusion models. *arXiv preprint*, 2023. 2
- [16] Jin-Young Kim, Hyojun Go, Soonwoo Kwon, and Hyun-Gyoon Kim. Denoising task difficulty-based curriculum for training diffusion models. *arXiv preprint arXiv:2403.10348*, 2024. 3
- [17] Diederik P Kingma. Auto-encoding variational bayes. *arXiv preprint arXiv:1312.6114*, 2013. 2
- [18] Mingxiao Li, Tingyu Qu, Ruicong Yao, Wei Sun, and Marie-Francine Moens. Alleviating exposure bias in diffusion models through sampling with shifted time steps. *arXiv preprint arXiv:2305.15583*, 2023. 3, 4
- [19] Senmao Li, Taihang Hu, Fahad Shahbaz Khan, Linxuan Li, Shiqi Yang, Yaxing Wang, Ming-Ming Cheng, and Jian Yang. Faster diffusion: Rethinking the role of unet encoder in diffusion models. *arXiv e-prints*, pages arXiv–2312, 2023. 2
- [20] Wenhao Li, Xiu Su, Shan You, Tao Huang, Fei Wang, Chen Qian, and Chang Xu. Not all steps are equal: Efficient generation with progressive diffusion models. *arXiv preprint arXiv:2312.13307*, 2023. 3
- [21] Enshu Liu, Xuefei Ning, Zinan Lin, Huazhong Yang, and Yu Wang. Oms-dpm: Optimizing the model schedule for diffusion probabilistic models. In *International Conference on Machine Learning*, pages 21915–21936. PMLR, 2023. 2
- [22] Jinming Lou, Wenyang Luo, Yufan Liu, Bing Li, Xinmiao Ding, Weiming Hu, Jiajiong Cao, Yuming Li, and Chengguang Ma. Token caching for diffusion transformer acceleration. *arXiv preprint arXiv:2409.18523*, 2024. 2
- [23] Cheng Lu, Yuhao Zhou, Fan Bao, Jianfei Chen, Chongxuan Li, and Jun Zhu. Dpm-solver: A fast ode solver for diffusion probabilistic model sampling in around 10 steps. *Advances in Neural Information Processing Systems*, 35:5775–5787, 2022. 2
- [24] Cheng Lu, Yuhao Zhou, Fan Bao, Jianfei Chen, Chongxuan Li, and Jun Zhu. Dpm-solver++: Fast solver for guided sampling of diffusion probabilistic models. *arXiv preprint arXiv:2211.01095*, 2022. 2
- [25] Zeyu Lu, Zidong Wang, Di Huang, Chengyue Wu, Xihui Liu, Wanli Ouyang, and Lei Bai. Fit: Flexible vision transformer for diffusion model. *arXiv preprint arXiv:2402.12376*, 2024. 1
- [26] Simian Luo, Yiqin Tan, Longbo Huang, Jian Li, and Hang Zhao. Latent consistency models: Synthesizing high-resolution images with few-step inference. *arXiv preprint arXiv:2310.04378*, 2023. 2
- [27] Xinyin Ma, Gongfan Fang, Michael Bi Mi, and Xinchao Wang. Learning-to-cache: Accelerating diffusion transformer via layer caching. *arXiv preprint arXiv:2406.01733*, 2024. 1, 2, 6, 7
- [28] Xinyin Ma, Gongfan Fang, and Xinchao Wang. Deepcache: Accelerating diffusion models for free. In *Proceedings of the IEEE/CVF Conference on Computer Vision and Pattern Recognition*, pages 15762–15772, 2024. 1
- [29] Mang Ning, Mingxiao Li, Jianlin Su, Albert Ali Salah, and Itir Onal Ertugrul. Elucidating the exposure bias in diffusion

- models. In *The Twelfth International Conference on Learning Representations*, 2023. 3, 4, 7
- [30] Mang Ning, Enver Sangineto, Angelo Porrello, Simone Calderara, and Rita Cucchiara. Input perturbation reduces exposure bias in diffusion models. In *International Conference on Machine Learning*, pages 26245–26265. PMLR, 2023. 3
- [31] Namuk Park and Songkuk Kim. How do vision transformers work? In *10th International Conference on Learning Representations, ICLR 2022*, 2022. 5
- [32] William Peebles and Saining Xie. Scalable diffusion models with transformers. In *Proceedings of the IEEE/CVF International Conference on Computer Vision*, pages 4195–4205, 2023. 1, 6
- [33] David Raposo, Sam Ritter, Blake Richards, Timothy Lillicrap, Peter Conway Humphreys, and Adam Santoro. Mixture-of-depths: Dynamically allocating compute in transformer-based language models. *arXiv preprint arXiv:2404.02258*, 2024. 1
- [34] Robin Rombach, Andreas Blattmann, Dominik Lorenz, Patrick Esser, and Björn Ommer. High-resolution image synthesis with latent diffusion models. In *Proceedings of the IEEE/CVF conference on computer vision and pattern recognition*, pages 10684–10695, 2022. 1
- [35] Tim Salimans and Jonathan Ho. Progressive distillation for fast sampling of diffusion models. *arXiv preprint arXiv:2202.00512*, 2022. 2
- [36] Pratheba Selvaraju, Tianyu Ding, Tianyi Chen, Ilya Zharkov, and Luming Liang. Fora: Fast-forward caching in diffusion transformer acceleration. *arXiv preprint arXiv:2407.01425*, 2024. 1, 2, 3, 6, 7
- [37] Yuzhang Shang, Zhihang Yuan, Bin Xie, Bingzhe Wu, and Yan Yan. Post-training quantization on diffusion models. In *Proceedings of the IEEE/CVF conference on computer vision and pattern recognition*, pages 1972–1981, 2023. 2
- [38] Junhyuk So, Jungwon Lee, Daehyun Ahn, Hyungjun Kim, and Eunhyeok Park. Temporal dynamic quantization for diffusion models. *Advances in Neural Information Processing Systems*, 36, 2024. 2
- [39] Jiaming Song, Chenlin Meng, and Stefano Ermon. Denoising diffusion implicit models. *arXiv preprint arXiv:2010.02502*, 2020. 2
- [40] Eleftherios Tsonis, Paraskevi Tzouveli, and Athanasios Voulodimos. Mitigating exposure bias in discriminator guided diffusion models. *arXiv preprint arXiv:2311.11164*, 2023. 3
- [41] A Vaswani. Attention is all you need. *Advances in Neural Information Processing Systems*, 2017. 1
- [42] Zhenyu Wang, Hao Luo, Pichao Wang, Feng Ding, Fan Wang, and Hao Li. Vtc-lfc: Vision transformer compression with low-frequency components. *Advances in Neural Information Processing Systems*, 35:13974–13988, 2022. 5
- [43] Felix Wimbauer, Bichen Wu, Edgar Schoenfeld, Xiaoliang Dai, Ji Hou, Zijian He, Artsiom Sanakoyeu, Peizhao Zhang, Sam Tsai, Jonas Kohler, et al. Cache me if you can: Accelerating diffusion models through block caching. In *Proceedings of the IEEE/CVF Conference on Computer Vision and Pattern Recognition*, pages 6211–6220, 2024. 1
- [44] Xingyi Yang, Daquan Zhou, Jiashi Feng, and Xinchao Wang. Diffusion probabilistic model made slim. In *Proceedings of the IEEE/CVF Conference on computer vision and pattern recognition*, pages 22552–22562, 2023. 2
- [45] Zhuoyi Yang, Jiayan Teng, Wendi Zheng, Ming Ding, Shiyu Huang, Jiazheng Xu, Yuanming Yang, Wenyi Hong, Xiaohan Zhang, Guanyu Feng, et al. Cogvideox: Text-to-video diffusion models with an expert transformer. *arXiv preprint arXiv:2408.06072*, 2024. 6, 7
- [46] Zhihang Yuan, Hanling Zhang, Pu Lu, Xuefei Ning, Linfeng Zhang, Tianchen Zhao, Shengen Yan, Guohao Dai, and Yu Wang. Ditfastattn: Attention compression for diffusion transformer models. *arXiv preprint arXiv:2406.08552*, 2024. 2, 6, 7
- [47] Dingkun Zhang, Sijia Li, Chen Chen, Qingsong Xie, and Haonan Lu. Laptop-diff: Layer pruning and normalized distillation for compressing diffusion models. *arXiv preprint arXiv:2404.11098*, 2024. 2
- [48] Qinsheng Zhang and Yongxin Chen. Fast sampling of diffusion models with exponential integrator. *arXiv preprint arXiv:2204.13902*, 2022. 2
- [49] Xuanlei Zhao, Xiaolong Jin, Kai Wang, and Yang You. Real-time video generation with pyramid attention broadcast. *arXiv preprint arXiv:2408.12588*, 2024. 6, 7
- [50] Chang Zou, Xuyang Liu, Ting Liu, Siteng Huang, and Linfeng Zhang. Accelerating diffusion transformers with token-wise feature caching. *arXiv preprint arXiv:2410.05317*, 2024. 6